JGR Planets

RESEARCH ARTICLE
10.1029/2019JE006252

Field-Aligned Photoelectron Energy Peaks at High Altitude and on the Nightside of Titan

Y.-T. Cao[1,2,3,4], A. Wellbrock[2,3], A. J. Coates[2,3], R. Caro-Carretero[2,3,5], G. H. Jones[2,3], J. Cui[4,6], M. Galand[7], and M. K. Dougherty[7]

[1]Key Laboratory of Lunar and Deep Space Exploration, National Astronomical Observatories, Chinese Academy of Sciences, Beijing, China, [2]Mullard Space Science Laboratory, Department of Space and Climate Physics, University College London, London, UK, [3]The Centre for Planetary Sciences at UCL/Birkbeck, London, UK, [4]School of Astronomy and Space Science, University of Chinese Academy of Sciences, Beijing, China, [5]Universidad Pontificia ICAI-ICADE Comillas, Madrid, Spain, [6]School of Atmospheric Sciences, Sun Yat-sen University, Zhuhai, China, [7]Department of Physics, Imperial College London, London, UK

Abstract The ionization of N_2 by strong solar He II 30.4-nm photons produces distinctive spectral peaks near 24.1 eV in Titan's upper atmosphere, which have been observed by the Electron Spectrometer (ELS) as part of the Cassini Plasma Spectrometer. The ELS observations reveal that, in addition to the dayside, photoelectron peaks were also detected on the deep nightside where photoionization is switched off, as well as at sufficiently high altitudes where the ambient neutral density is low. These photoelectron peaks are unlikely to be produced locally but instead must be contributed by transport along the magnetic field lines from their dayside source regions. In this study, we present a statistical survey of all photoelectron peaks identified with an automatic finite impulse response algorithm based on the available ELS data accumulated during 56 Titan flybys. The spatial distribution of photoelectron peaks indicates that most photoelectrons detected at an altitude above 4,000 km and a solar zenith angle above 100° are field aligned, which is consistent with the scenario of photoelectron transport along the magnetic field lines. Our analysis also reveals the presence of a photoelectron gap in the deep nightside ionosphere where almost no photoelectrons were detected. It appears to be very difficult for photoelectrons to travel to this region, and such a feature may not be driven by the changes in the orientation between the solar and corotation wakes.

Plain Language Summary The strong solar Extreme Ultraviolet radiation generates photoelectrons with spectral peaks near 24.1 eV in the Titan's dayside ionosphere, which have been observed by the Electron Spectrometer (ELS), part of the Cassini Plasma Spectrometer. In addition to the dayside, ELS also detected photoelectron peaks on the nightside where solar radiation is switched off and at large distances from Titan where the ambient neutral density is extremely low. These photoelectron peaks are, therefore, more likely contributed by transport along the magnetic field lines from the dayside. We present a statistical survey of all photoelectron peaks identified with an automatic algorithm based on the available ELS data. Our analysis confirms that most photoelectrons detected at high altitudes and in the deep nightside move along magnetic field lines. Besides, our result reveals, for the first time, the presence of a photoelectron gap on the nightside. However, no viable mechanism, such as the Saturn local time variation, could explain the gap.

Key Points:
- Based on an automatic algorithm, we present a statistical survey of photoelectron energy peaks observed during 56 Titan flybys
- Most photoelectrons detected at an altitude >4,000 km and a solar zenith angle >100° are field aligned
- We identify a region on the dark-side (≥130° SZA) where almost no photoelectrons were observed

Correspondence to:
Y.-T. Cao,
caoyt@nao.cas.cn

Citation:
Cao, Y., Wellbrock, A., Coates, A. J., Caro-Carretero, R., Jones, G. H., Cui, J., et al. (2020). Field-aligned photoelectron energy peaks at high altitude and on the nightside of Titan. *Journal of Geophysical Research: Planets*, *125*. https://doi.org/10.1029/2019JE006252

Received 25 OCT 2019
Accepted 3 DEC 2019

1. Introduction

Titan is the largest moon of Saturn and lacks a significant intrinsic magnetic field but has a dense neutral nitrogen-methane atmosphere (Backes et al., 2005; Cui, Yelle, et al., 2009; Neubauer et al., 1984). Within its atmosphere, an ionosphere is formed at altitudes above 400 km with an ionospheric peak varying between 950 and 1,250 km on the dayside and between 900 and 1,400 km on the nightside (Ågren et al., 2009). Titan is usually immersed in Saturn's magnetosphere because the semimajor axis of Titan's orbit is about 20 Saturn radii. Thus, besides solar radiation, Saturn's magnetospheric plasma contributes as a source of Titan's ionosphere (Agren et al., 2007; Cravens et al., 2009). Titan has been occasionally observed in Saturn's magnetosheath and supersonic solar wind (Bertucci et al., 2008, 2015; Ma et al., 2009). It also acts as a source of particles for Saturn's magnetosphere. For example, Titan's ionospheric ions can be picked up by incoming

magnetospheric plasma, which causes mass loading in the upstream flowing plasma (e.g., Coates, 2009; Hartle et al., 2006; Regoli et al., 2016). Mass loading and magnetic pressure forces contribute to the external magnetic field draping around Titan's conducting ionosphere, also resulting in the formation of a tail downstream of the corotation flow (e.g., Backes et al., 2005). The relative position between this magnetotail (also known as corotation wake) and the solar wake (i.e., nightside) depends on Titan's orbital position and changes continuously (Ness et al., 1982).

In planetary atmospheres, photoionization is an important source of ionization. Photoelectrons with a particular energy can be produced by the solar Extreme Ultraviolet (EUV) and X-ray ionization of various molecules in the sunlit ionospheres (Coates et al., 2011). The He II 30.4-nm line is one of the most intense EUV lines in solar radiation. It produces photoelectrons with different energy peaks in the ionospheres of different planets in the solar system, depending on the main neutral composition in the upper atmosphere. For instance, the photoelectron spectrum contains distinctive peaks at 24–25 eV or at ~22 eV associated with the ionization of N_2 or O at Earth (e.g., Coates et al., 1985; Nagy & Banks, 1970). At both Mars and Venus, photoelectrons with energy peaks at ~22 and ~27 eV are observed due to the ionization of CO_2 or O (e.g., Coates et al., 2008; Cui et al., 2011; Mantas & Hanson, 1979; Schunk & Nagy, 2000).

At Titan, photoelectrons with an energy peak at ~24.1 eV are produced by the ionization of N_2 with the He II 30.4-nm line radiation (e.g., Coates et al., 2007, 2011; Cui, Galand, et al., 2009; Galand et al., 2006, 2010). The Electron Spectrometer (ELS), part of the Cassini Plasma Spectrometer (CAPS), has observed these photoelectrons as a discrete peak in the electron energy spectrum during Titan flybys of the Cassini-Huygens mission (Young et al., 2004). Instead of being observed at 24.1 eV, the photoelectron discrete peaks in the electron energy spectrum are slightly shifted due to the spacecraft potential and the ambiopolar electric field. The spacecraft potential is typically 0 to −2 V when Cassini passes through Titan's ionosphere (e.g., Coates et al., 2007; Wahlund et al., 2005). The upper limit of Titan's ambipolar electric field, between the sunlit ionosphere and up to 6.8 Titan radii, is 2.95 eV (Coates, Wellbrock, Waite, et al., 2015). Thus, the 24.1-eV photoelectrons are virtually always seen in the 22.2-eV ELS energy bin. At distances higher than ~2,000 km, CH_4 becomes more abundant than N_2 in Titan's atmosphere (Cui et al., 2012; Strobel, 2012), and the photoelectron produced by single, non-dissociative ionization of CH_4 with the He II line radiation has an energy of 28.2 eV (Liu & Shemansky, 2006). Besides the observations of photoelectron peaks with an energy of 24.1 eV in the sunlit ionosphere, where they were produced, these photoelectrons have also been detected on the nightside and at high altitudes of Titan (Coates et al., 2007; Wellbrock et al., 2012). The lack of solar EUV radiation on the nightside and the low neutral N_2 density at large distances from Titan mean that these observed photoelectrons are less likely to be produced locally. The most likely explanation is that these hot electrons were escaping the low-altitude sunlit ionosphere of Titan, traveling along magnetic field lines (Coates et al., 2007, 2015; Wei et al., 2007). Wellbrock et al. (2012) compared the Cassini data with the results from a global quasi-neutral hybrid model of Titan's interaction with Saturn's magnetosphere. They found that for the T15 flyby, there were magnetic field lines connecting the sunlit ionosphere and the location crossed by Cassini where photoelectrons were observed. This explains the presence of photoelectrons on the nightside of Titan.

Studying photoelectron detections outside the sunlit ionosphere of Titan can therefore improve our understanding of the complex spatial distribution of the magnetic field line geometry and plasma morphology in Titan's space environment. Similar works have been undertaken to determine the Martian magnetic topology based on the observations of photoelectron peak by the Mars Express mission (Frahm et al., 2006) and the Mars Atmosphere and Volatile Evolution mission (e.g., Xu et al., 2016; Xu, Mitchell, Liemohn, et al., 2017; Xu, Mitchell, Luhmann, et al., 2017).

In this study, we examine the ELS data from 56 Titan flybys to present a statistical survey of all observed 24.1-eV photoelectrons produced by the ionization of N_2 with the He II line radiation. In section 2, we start with a brief description of the ELS data set we used. We present a typical photoelectron detection in Titan's nightside ionosphere in section 3.1 and the spatial distribution of all photoelectron peak detections from all available Titan flybys, focusing on the nightside, in section 3.2, where we also find that there is a region on the dark-side where virtually no photoelectron peaks. This is followed by section 3.3 where we define an anisotropy factor in terms of the photoelectron pitch angle distributions (PADs) of the photoelectrons to classify the results. In section 4, we discuss the results, their implications, and also the possible mechanisms

Table 1
Summary of the Cassini Titan Flybys Studied Here

Flyby	Date	LT (hr)	LT type[a]	Flyby	Date	LT (hr)	LT type
TB	13-Dec-04	10.47	c	T33	29-Jun-07	13.53	c
T3	15-Feb-05	10.33	c	T34	19-Jul-07	18.8	d
T4	31-Mar-05	5.27	b	T35	31-Aug-07	11.53	c
T5	16-Apr-05	5.27	b	T36	2-Oct-07	11.47	c
T6	22-Aug-05	5	b	T37	19-Nov-07	11.4	c
T7	7-Sep-05	4.93	b	T40	5-Jan-08	11.33	c
T8	28-Oct-05	9.27	c	T41	22-Feb-08	11.2	c
T10	15-Jan-06	8.47	b	T42	25-Mar-08	11.13	c
T11	27-Feb-06	1.13	a	T43	12-May-08	11	c
T12	19-Mar-06	6.4	b	T44	28-May-08	10.93	c
T13	30-Apr-06	23.13	a	T45	31-Jul-08	11	c
T14	20-May-06	4.4	b	T46	3-Nov-08	10.5	c
T15	2-Jul-06	21.2	a	T47	19-Nov-08	10.5	c
T16	22-Jul-06	2.4	a	T48	5-Dec-08	10.5	c
T17	7-Sep-06	2.27	a	T49	21-Dec-08	10.4	c
T18	23-Sep-06	2.27	a	T51	27-Mar-09	10	c
T19	9-Oct-06	2.2	a	T52	4-Apr-09	22	a
T20	25-Oct-06	2.13	a	T55	21-May-09	22	a
T21	12-Dec-06	2	a	T56	6-Jun-09	22	a
T23	13-Jan-07	1.93	a	T58	8-Jul-09	22	a
T24	29-Jan-07	1.87	a	T59	24-Jul-09	22	a
T25	22-Feb-07	13.8	c	T61	25-Aug-09	21.8	a
T26	22-Feb-07	13.8	c	T62	12-Oct-09	21.7	a
T27	26-Mar-07	13.73	c	T63	12-Dec-09	17	d
T28	10-Apr-07	13.67	c	T64	28-Dec-09	17	d
T29	26-Apr-07	13.67	c	T65	12-Jan-10	17	d
T30	12-May-07	13.6	c	T69	5-Jun-10	16	d
T32	13-Jun-07	13.53	c	T71	7-Jul-10	16.04	d

Note. Date, local time (LT), and local time type are shown for each flyby.
[a]LT type indicates the relative position of solar and corotation wake (see section 4).

responsible for the gap region on the dark-side and the criteria of the anisotropy factor. Finally, we provide concluding remarks in section 5.

2. Instrumentation and Data

The CAPS-ELS is a top-hat hemispherical electrostatic analyzer which measures the energy and angle distribution of electrons. It works by sweeping a 63 level energy spectrum from 28,000 to 0.6 eV every 2 s. The energy bins are logarithmically spaced with an energy resolution ($\Delta E/E$) of 16.7% (Linder et al., 1998; Young et al., 2004). ELS has eight sectors ("anodes") with 20° × 5° angular coverage and has a total instantaneous angular coverage of 160° × 5°. The CAPS-ELS is fixed to a rotating platform, or actuator, rotating around the Z axis of the spacecraft by ±104°, with which approximately 56% of full 4π sky can be covered in 3 min (Lewis et al., 2008; Young et al., 2004). In this study we only use Anodes 2–7 because Anodes 1 and 8 are affected by considerable spacecraft-plasma interactions (Lewis et al., 2010).

Our work is based on the electron spectra data acquired by ELS during 56 Titan encounters, from December 2004 to July 2010. The flyby details are shown in Table 1. We use an automatic finite impulse response algorithm, which is based on a short-term-average/long-term-average phase picker (Allen, 1978, 1982), to find 24.1-eV photoelectron peaks in the ELS data. The algorithm calculates a characteristic function for an averaged spectrum every three sweeps (6 s) twice and examine the characteristic function to see if it

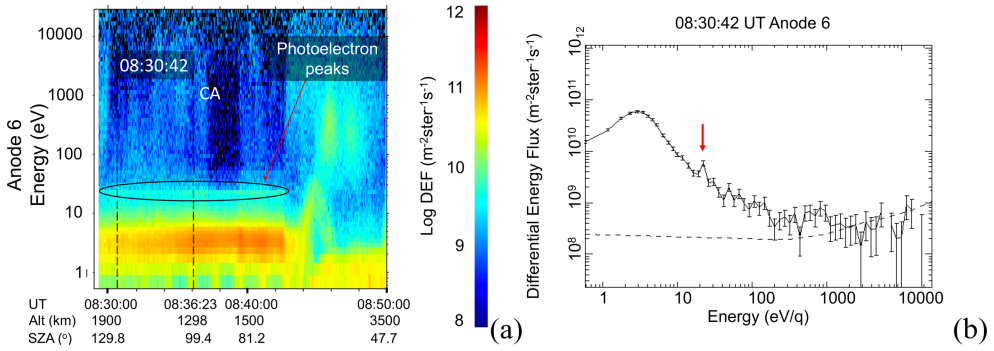

Figure 1. An example of ELS data from T62 on 12 October 2009. (a) ELS energy-time spectrogram from Anode 6. The prominent ionospheric photoelectron peak near 24.1 eV is visible from 08:29 UT to 08:43 UT. The dashed lines indicate the time of the closest approach (CA) and the time of the spectrum used in panel (b), respectively. (b) Electron spectrum averaged over three energy sweeps (6 s) at 08:30:42 UT. The arrow points at the center of the 22.2-eV energy bin which contains the 24.1-eV photoelectron peak. Error bars assume Poissonian statistics on the original data.

meets the criteria for the characteristic function of photoelectrons. A quality index is then determined based on the signal-to-noise ratio. All photoelectron identification results can be accessed via Caro-Carretero, Raquel; Wellbrock, Anne; Cao, Yutian (2019), "Cassini ELS Photoelectron identification," Mendeley Data, v1 (https://doi.org/10.17632/dwxhzbnvr9.1).

We further classify the photoelectron observations according to their PAD. Pitch angle is the angle between the electron velocity and the magnetic field direction and indicates the direction of the electron propagation that moves along the magnetic field line. According to the PAD, we are able to determine if the photoelectrons are observed close to their source region (a more isotropic PAD) or moved a long way from it (a more field-aligned PAD). For field-aligned electrons, the pitch angle direction with the maximum flux (PA_{max}) should be close to 0° or 180° . The PAD is determined based on the Cassini magnetometer (MAG) data (Dougherty et al., 2004). Similar to the spectrum, we averaged the PAD every three sweeps (6 s) and resample the PAD covered by Anodes 2–7 into 10° pitch angle bins. Due to the field of view (FOV) limitations, a full 180° coverage is almost never reached, and we classify the photoelectrons with PAD coverage spanning more than 90° as the sufficient angular coverage category. An additional requirement for this category is that there is some pitch angle coverage at pitch angles <40° or >140° to ensure that coverage is sufficient to observe field-aligned PADs (parallel or antiparallel) when present. More details will be discussed in section 3.

3. Observations and Analysis

3.1. Typical Photoelectron Peaks in Titan's Ionosphere: An Example

As a large number of photoelectrons with an energy peak at ~24.1 eV are generated in Titan's ionosphere, a clear discrete peak of these photoelectrons can be seen in the electron energy spectrum from CAPS-ELS. In Figure 1a, we present a typical CAPS-ELS energy-time spectrogram during the T62 flyby, which occurred on 12 October 2009 with closest approach at an altitude of 1,298 km at 08:36:23 UT. Here we only show the data from Anode 6. The spacecraft is in the ionosphere from 08:29 UT till 08:43 UT when the hot, dense electrons are the prominent feature in the spectrogram. A photoelectron peak at 24.1 eV is visible as a fine, subtle line during this period. After 08:43:32 UT, Saturn's magnetospheric electrons, with energy of a few hundred electron volt, appear highly variable, and the population of spacecraft photoelectrons with energy <5 eV can be observed as a result of the spacecraft being positively charged.

Figure 1b presents an electron spectrum averaged over three energy sweeps (i.e., 6 s) and with a starting time stamp at 08:30:42 UT during the T62 flyby. The broad peak below 10 eV is the hot ionospheric electrons and the arrow points at the photoelectron peak that lies in the energy bin of 22.2 eV. Because the energy resolution of ELS ΔE/E is 16.7%, the 22.2-eV energy bin contains 24.1 eV, the theoretical energy of the primary photoelectrons produced by the ionization of N_2 by HeII (30.4 nm). Error bars assume Poissonian statistics on the original data.

From 08:29 UT to 08:38 UT, the solar zenith angle (SZA) decreases from 130° to 90° , which indicates that Cassini was in the nightside ionosphere. During this period, the photoelectron peak at 24.1 eV is visible all the time. At these SZAs we would expect the solar radiation to be weak or nonexistent. It is therefore

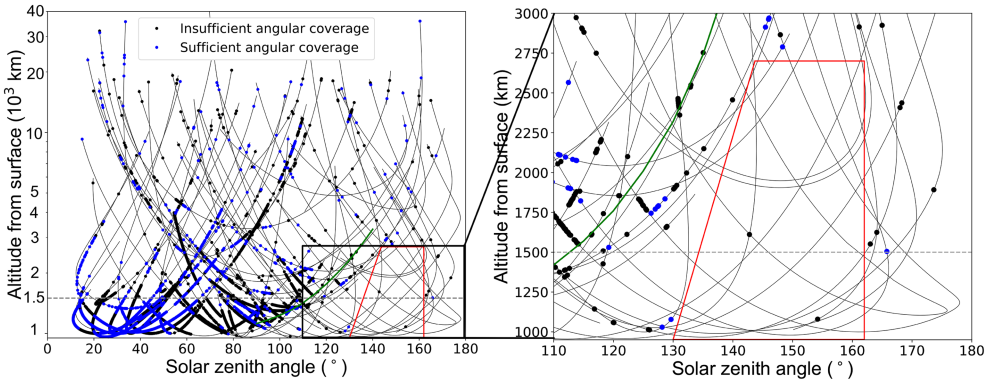

Figure 2. Photoelectron peaks detected by Cassini CAPS-ELS during 56 Titan encounters. Every dot is an observation, and the lines show the Cassini trajectory. (a) A general view of the spatial distribution of all observed photoelectron peaks. Altitude is given in kilometers, measured from Titan's surface, and is shown on a log scale. The blue and black data points indicate the photoelectron peaks with sufficient angular coverage (PAD angular coverage >90°) or insufficient angular coverage (PAD angular coverage ≤90°), respectively. (b) Zoomed-in version of Figure 2a, with 950 km < Alt < 3,000 km and SZA ranges >110°. Altitude is shown on a linear scale. The green line indicates the He II radiation edge, beyond which the He II radiation intensity goes below 10%. The grey dashed line presents the exobase altitude, above which the photoelectron collisions with ambient neutral particles become negligible. The region enclosed by the red trapezoid only shows two data points observed at 19:40:51 UT during T5 (the upper one) and 21:24:04 UT during T55 (the bottom one).

less likely for the 24.1-eV photoelectron to be produced locally, especially with such a relatively high abundance. This encounter is therefore an example of 24.1-eV photoelectron observations that are likely to have been produced remotely at a lower altitude on the sunlit side and traveled to the observation site along magnetic field lines. We can use photoelectron peak observations in this fashion to learn more about the spatial distribution of surrounding magnetic field lines.

3.2. SZA-Alt Distribution of Photoelectron Peaks

Using the automatic finite impulse response algorithm, we detected photoelectrons with a peak near 24.1 eV during each of the 56 flybys in the ELS data. In Figure 2, we present the spatial distribution of photoelectrons according to the SZA and altitude of the location where ELS observed these photoelectrons. Each dot represents a single detection while the lines are the trajectory of Cassini during each flyby. Because the PAD of each photoelectron observation spans less than 180° , we classified the photoelectrons with PAD angular coverage over 90° as sufficient angular coverage category (shown as blue dots) and the photoelectrons with PAD angular coverage less than 90° as insufficient angular coverage category (shown as black dots); 65% of the photoelectron peaks are found under 2,000 km and at a SZA less than 90°, that is in the sunlit ionosphere, where most 24.1-eV photoelectrons are primarily produced through the ionization of neutral N_2 with the He II solar line radiation. The altitude of the observed photoelectrons varies from 950 to 40,000 km while the SZA ranges from 10° to 170°. The grey dashed line indicates the photoelectron exobase of Titan, located at the altitude of ~1,505 km. The exobase, above which the photoelectron collisions with ambient neutral particles become negligible, is estimated as the altitude where the mean path length is equal to the pressure scale height. Based on the neutral density adapted from Strobel (2012), we provide an estimated He II line radiation edge, shown as the green line, below which the He II radiation intensity is less than 10% of the subsolar value. The He II radiation edge is determined by integrating the photo-absorption of the He II line radiation by the atmosphere, assuming a spherical atmosphere and adopting N_2 is the only neutral component. Due to lack of sufficient neutral density data, we only determined the He II radiation edge up to 3,300 km.

In this work we focus on the nightside ionosphere region. We therefore zoom in Figure 2a and present the region over the altitude range of 950–3,000 km and with the SZA beyond 110° in Figure 2b. The peak electron density of Titan's atmosphere lies at approximately 1,200 km, and the ionosphere can extend up to nearly 2,200 km (Ågren et al., 2009; Galand et al., 2014). Beyond 110° SZA the solar He II 30.4-nm flux is almost attenuated, which no longer generates substantial photoelectrons in the main ionosphere (Galand et al., 2010). The 24.1-eV photoelectrons found below the green line in Figure 2b, where the He II radiation is relatively low, cannot have been produced locally. These observations indicate that there may be magnetic

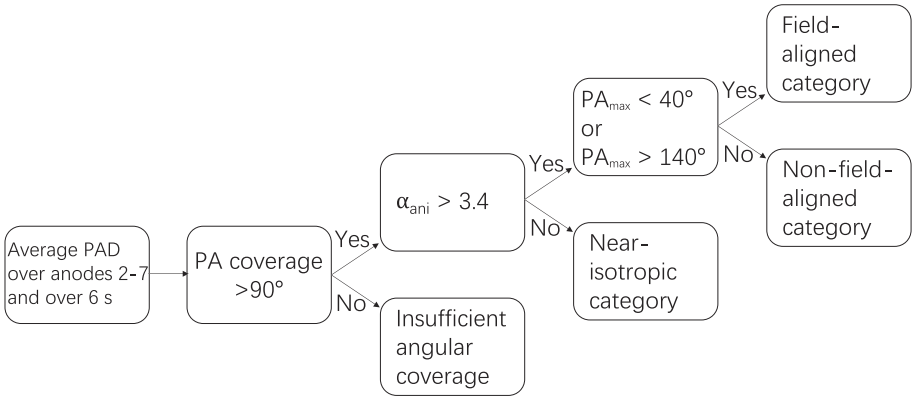

Figure 3. Fan plots of the electron PAD observed at two different times. The energy shown on the *X* and *Y* axes increases radially outwards from the center of each plot. The color scale indicates the differential energy flux (DEF) of electrons along a given radial direction associated with a given pitch angle bin. Because of the spacecraft negative potential combined with the energy resolution of the energy grid, photoelectron peaks at 24.1 eV were found in the 22.2-eV energy bin in both cases. Left panel (a) shows data from the T5 flyby at 19:40:51 UT, corresponding to the dot in the trapezoid-shaped region in Figure 2b. As DEF differences among the electrons with different pitch angles are less than half magnitude, the PAD of (a) appears to be nearly isotropic. The right panel (b) shows the observation at 08:30:42 UT during T62, corresponding to the spectrum in Figure 1b. This observation happened in the nightside ionosphere, and the PAD shows that the photoelectrons are field aligned.

field lines that connect the nightside and the dayside ionosphere. The connections can sometimes reach the deep nightside with SZA above 170°.

In addition, we find a trapezoid-shaped gap area in the middle of Figure 2b with SZA >130° at an altitude range between 950 and 2,700 km. In this region only two photoelectron detections, the dots in Figure 2b at 1,611 km, SZA = 143° and at 1,070 km, SZA = 154°, were identified. Except for these two observations, no photoelectron peaks were detected during the other 20 Titan flybys which passed through this region.

The detection in the gap region at 1,611 km was observed during T5 at 19:40:51 (UT). The T5 encounter occurred on 16 April 2005, and the spacecraft flew through the nightside. We examine the PAD of this detection to see if photoelectrons observed here were moving along magnetic field lines. Figure 3 shows fan plots at two different times showing the PAD of electrons averaged over 6 s (three energy sweeps) and resampled into 10° pitch angle bins. The energy increases radially outwards from the center of the plot, shown on the *X* and *Y* axes. Only three energy bins are shown here. The central energy of the three energy bins are 19.26, 22.2, and 26.34 eV, respectively. The color indicates the differential energy flux (DEF) of electrons along that direction, and each angle bin covers 10°. The 24.1-eV photoelectron peak is detected in the 22.2-eV energy bin.

Figure 3a is the PAD of the electrons detected at 19:40:51 (UT) during T5. From Figure 3a we can see that most of the electrons were observed at pitch angles between 80° and 90°, perpendicular to the magnetic field. The DEF differences among the electrons with different pitch angles are less than 60%. Unfortunately, the data only covered pitch angles between 60° and 140° due to the FOV restriction. Thus, we do not know how many electrons are parallel to the magnetic field, and it is difficult to distinguish between field-aligned and non-field-aligned photoelectrons in this case. The PAD still indicates that these photoelectrons may be near isotropic. Usually newly born photoelectrons are expected to have isotropic PAD (e.g., Galand et al., 2006). The PAD coverage of the other photoelectron peak observation in the gap region is only 20° , making it difficult to identify whether it is field aligned or not.

We also show the PAD of electrons which the ELS detected at 08:30:42 UT during T62 (see Figure 1b) in Figure 3b. The pitch angle observations at this time of the flyby cover a range of 20° to 130° . The DEF of photoelectrons with low pitch angles is over three times higher than that of photoelectrons perpendicular to the magnetic fields. This means that photoelectrons detected at this time appears strongly field aligned. These photoelectrons are highly likely to have moved along magnetic field lines to the nightside ionosphere where they were detected.

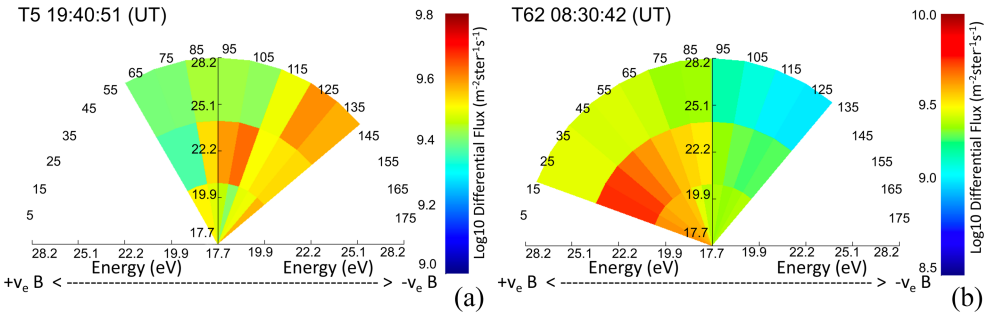

Figure 4. Flowchart of the way that we classify photoelectrons using their PAD data. PA_{max} is the pitch angle direction with the maximum DEF.

3.3. Anisotropy Factor

Here we define an anisotropy factor, α_{ani}, to classify photoelectron detections into three types: near isotropic, field aligned, and non-field aligned. For the PAD of electrons seen in the 22.2-eV ELS energy bin, we calculate an anisotropy factor α_{ani}, defined as the ratio of the maximum DEF among all angular bins to the minimum DEF as

$$\alpha_{ani} = \frac{DEF_{max}}{DEF_{min}}.$$

Strictly speaking, the pitch angle data contain all electrons detected by the ELS, but in this energy bin photoelectrons are usually the dominant source. Figure 4 shows a flow chart we use to classify different types of photoelectrons using our anisotropy factor. We use PAD data averaged over Anodes 2–7 and over three energy sweeps (6 s). The α_{ani} are only calculated for photoelectrons with sufficient pitch angle coverage (the blue dots shown in Figure 1). Though about 80% of photoelectrons are not classified due to this angular coverage criterion, the remaining 1,328 data points distribute uniformly (see Figure 1) and are adequate for further analysis. If $\alpha_{ani} \leq 3.4$ we define the photoelectron distributions as near isotropy, because it indicates that the DEF of photoelectrons are similar regardless of the PAD. $\alpha_{ani} > 3.4$ means that the majority of photoelectrons have a preferred pitch angle, which correspond to the bin with the largest DEF. Anisotropic distributions are further classified as field aligned ($PA_{max} < 40°$ or $PA_{max} > 140°$) or not field aligned ($40° < PA_{max} < 140°$). Based on these definitions, the two PADs in Figures 3a and 3b are classified as insufficient pitch angle coverage and field aligned, respectively. Because of the FOV limitation and the precision of the data, we chose the threshold value $\alpha_{ani}^{limit} = 3.4$, a relatively large value, as the criterion to distinguish the near-isotropic and anisotropic photoelectron angular distributions. Changing the threshold value of α_{ani}^{limit} may affect the classification of the photoelectrons, and we discuss this further in section 5.

We use the anisotropy factor to identify whether photoelectrons observed by the ELS are far away from the region where they were primarily produced due to photoionization. In Figure 5, we present histograms of probability of each type of photoelectron angular distributions in fixed altitude bins below 14,000 km. Each altitude bin contains at least 10 photoelectron observations to ensure statistical significance. We define the probability of detection as the ratio of the number of photoelectron peak detections to the total number of samples with sufficient pitch angle coverage in the ELS 22.2-eV energy bin. The total number of samples for one flyby means the number of every single energy sweep from the time when the first photoelectron peak was observed to the time of the last photoelectron peak signal.

The top panel in Figure 5 shows the probability of the three types of photoelectrons in 2,000-km altitude bins. Below 2,200 km, where Titan's main ionosphere is located, most of the observed photoelectron peaks on the dayside are expected to be locally produced and to have an isotropic angular distribution (Galand et al., 2006). The probability of detection of the near-isotropic photoelectrons is the highest, over 21%. The sum of the observation probability for the three types of photoelectrons is not 100% as the ELS did not always observe photoelectrons throughout each encounter. Because we define every flyby time period as the time interval between the first and last photoelectron detections, closest approach variations among different flybys affect the altitude range sampled strongly. In this work, we are only interested in the relative probabilities of the three types of photoelectron angular distributions. With increasing altitude, the ratio of the probability of field-aligned photoelectron distribution to that of other distributions increases. Above

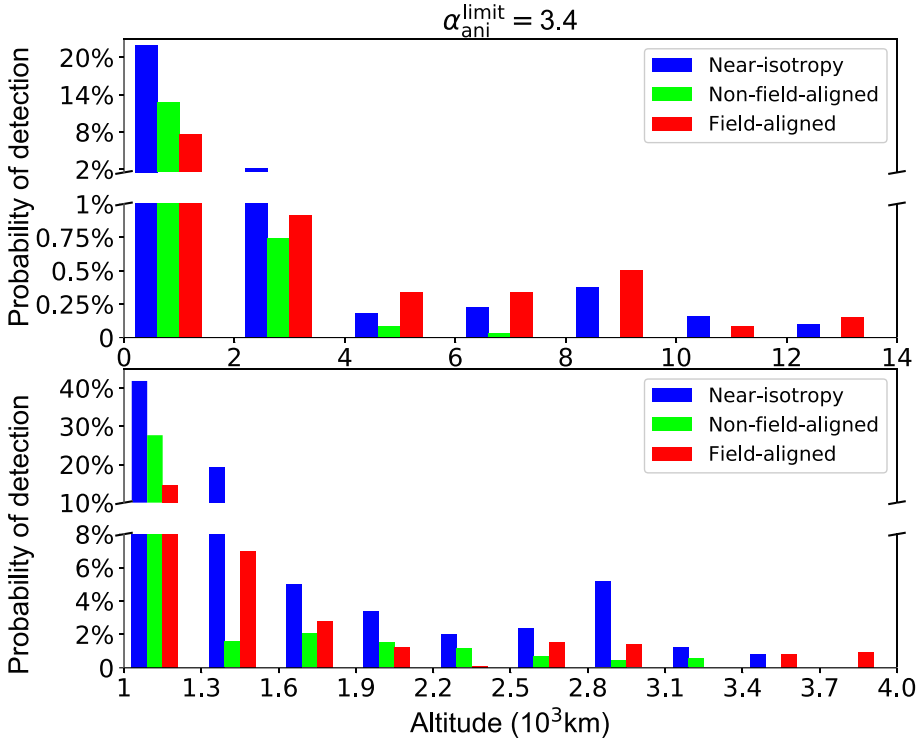

Figure 5. Histograms of the detection probability of three types of photoelectron angular distributions during a total of 56 flybys at a fixed height bin. The probability of detection of a given angular distribution class is the ratio of the number of detections for this class to the number of total samples in the 22.2-eV energy bin. The top panel shows the detection probability for every 2,000-km altitude bin below 14,000 km, and the bottom panel shows the probability between 1,000 and 4,000 km for every 300-km bin. The *Y* axis is nonuniform and emphasizes the significant variation of the detection probability with increasing altitude.

4,000 km, field-aligned photoelectron distributions become the most likely to be observed, because the photoelectrons are expected to travel to the observation sites via magnetic field lines, resulting in more field-aligned angular distributions.

In Figure 5b, we zoom in to an altitude range between 1,000 and 4,000 km and determine the probabilities of each class in 300-km altitude bins. The near-isotropic category is always dominant in this altitude range, indicating that photoionization generates a substantial amount of photoelectrons below 4,000 km. Below 1,300 km, the detection probability of non-field-aligned photoelectrons is about twice higher than that of field-aligned photoelectrons. This is in line with our expectation to see less field-aligned photoelectrons because some of them may travel away along magnetic field lines easily. Above 1,300 km, which is above the ionospheric peak, the replenishment of photoelectrons via transport along magnetic field lines becomes much more important, and the detection probability of field-aligned photoelectrons is therefore higher than that of non-field-aligned photoelectrons.

Figure 6 presents a similar histogram to Figure 5, but showing the probability of detecting the three types of photoelectron angular distributions as a function of SZA using 20° SZA bins. On the dayside (SZA < 90°), where most photoelectrons are produced locally, the near-isotropic photoelectron distributions are also the dominant type except for the SZA range between 20° and 40° . For SZA beyond 100° , the field-aligned photoelectron distribution becomes the most probable type to be observed, indicating that on the nightside the observed photoelectrons are likely to have traveled along magnetic field lines before being detected by the ELS. Above 120° , the total probability of observing photoelectrons decreases sharply to below 0.3%. Over the SZA range of 0°–20° , though the near-isotropic photoelectrons are the most likely to be observed, the detection probability of near-isotropic photoelectrons is only slightly higher than field-aligned photoelectrons. Between 20° and 40° , the detection probability of near-isotropic photoelectrons is even lower than non-field-aligned photoelectrons. The above counterintuitive scenario indicates that the SZA variation of

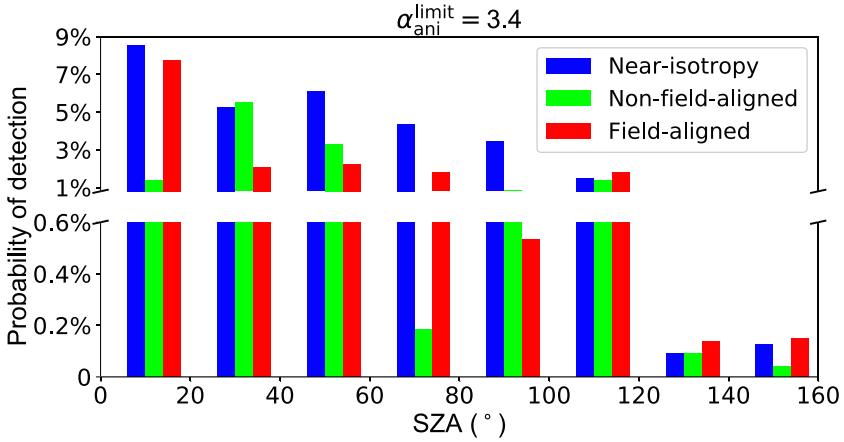

Figure 6. Similar to Figure 5, but as a function of SZA using 20° SZA bin.

photoelectron PAD may not only depend on the solar radiation input. More detailed case studies in this region are required to help explain this slightly contradicting trend.

4. Discussion

We have presented the spatial distribution of the 24.1-eV photoelectron peaks detected by the ELS during 56 Titan encounters in section 3; 65% of the photoelectrons are seen in the dayside ionosphere, where they were produced. In other regions, at high altitude or on the nightside, there were also some detections. Photoelectrons found in these regions traveled there from the sunlit ionosphere along magnetic field lines (Coates et al., 2007; Wellbrock et al., 2012). Detections of the photoelectrons show that draped magnetic field lines extend to extremely high altitudes and deep into the nightside. However, there is a large photoelectron gap found in the dark-side as illustrated in Figure 2b. The lack of photoelectrons in this region indicates that the magnetic field lines, which connect to the lower sunlit ionosphere, do not appear to be connected to this gap region. This may be caused by the specific orientations of the solar and corotation wakes. As Titan orbits Saturn, the solar radiation input and plasma flow input are not always overlapping. Solar EUV radiation produces photoelectrons in Titan's sunlit ionosphere, while Saturnian magnetic field lines draped around Titan, roughly with respect to the corotation direction (Bridge et al., 1981; Coates et al., 2007, 2011; Galand et al., 2006). Sillanpää et al. (2006) used a hybrid simulation to investigate the effects of the orbit position on magnetic interaction with Titan's plasma. They found that the number density of exospheric ions in shadow changes with local time (LT).

In Figure 7, we present sketches of configurations of solar radiation and draped magnetic field lines around Titan at different LTs. Saturn's nominal magnetospheric plasma flow is always coming from the left while solar shadowed area changes on Titan in this figure. Because the magnetic pressure is comparable to thermal pressure in the exo-ionosphere region, above approximately 1,430 km from Titan surface, plasma flow is not always from day to night (Agren et al., 2007; Cravens et al., 2009). When the solar wake and corotation wake are in an antiparallel position, like in Figure 7b, the field line geometry may only favor electron transport from dayside terminator region to nightside terminator region. The photoelectrons will be lost quickly once the field lines dip into the dense atmosphere at high SZAs. Thus, it is difficult for photoelectrons to travel along magnetic field lines to the deep nightside. In Figure 7a, it should be easier for photoelectrons produced on the flow side (the top hemisphere) to transport to the nightside ionosphere and to be observed by Cassini than the photoelectrons produced on the wake side (the bottom hemisphere). A similar tendency is expected in Figure 7c. Only for Figure 7d, the photoelectrons produced on the dayside may be transported to the nightside along magnetic field lines more easily.

We further add the photoelectron observations in Figure 2 onto Figure 7 according to the LT during each flyby; for example, the observations during LT 21:00 to 03:00 are plotted in Figure 7a. The LT type of each flyby is listed in Table 1. Similar to Figure 2, the grey lines, green lines, and the red trapezoid regions in Figure 7 represent the Cassini trajectories, He II radiation edge, and the photoelectron gap region, respectively. The wake-side and flow-side flybys are separated in Figures 7a and 7d. Photoelectrons can be observed

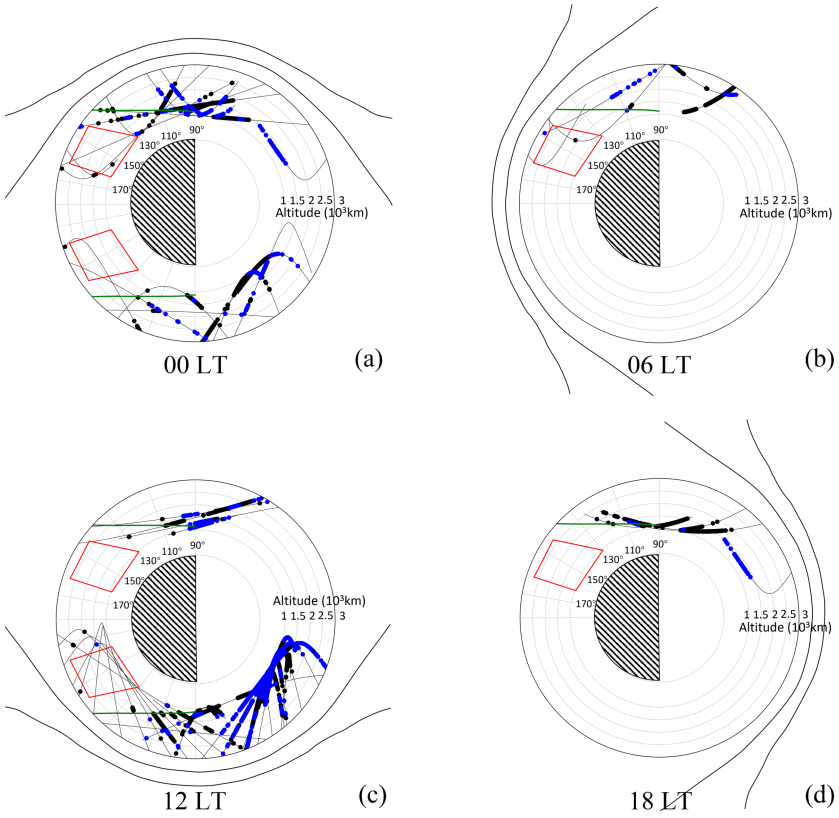

Figure 7. Sketches of the idealized draped magnetic field lines near Titan during four different local times (LTs) of Titan with respect to Saturn. Black lines are draped magnetic field lines. The shadowed surface on Titan is shown as a shaded area (dark-side). The sketches are shown in Titan's orbital plane, assuming that the Sun is always at the right of Titan. Saturn's nominal magnetospheric corotation flow therefore changes with different LTs. The results in Figure 2 are presented in four panels, including the observed photoelectron events, grey Cassini trajectories, green He II radiation edge, and the red trapezoid gap, according to the LT during each flyby (see Table 1 for the classification).

below the HeII edge during all four types of conditions, and we found the a, b, and c type of orientations in the gap area where almost no photoelectrons are detected. For the type a or type c situation, ELS was able to measure photoelectrons whenever Cassini passed through the flow side or wake side. The T5 and T55 flybys, during which the photoelectrons were detected in the gap region, took place at the LT of 22:00 and 05:16, respectively. The results in Figure 7 appear to be inconsistent with our previous discussion; thus, we cannot simply use this generalized classification and the configuration of solar wake and corotation wake to explain the photoelectron transport and the presence of the gap in Titan's ionosphere. Maybe there are some photoelectrons but the flux is not high enough to create a peak during most of gap flybys, or maybe their energy changed because of scattering process or other mechanism (Coates, Wellbrock, Frahm, et al., 2015; Tsang et al., 2015). Some case studies in the gap region are required, which is beyond the scope of this study but will be the focus of future studies.

The observation of near-isotropic photoelectrons at high altitude (above 8,000 km in Figure 5a) or on the nightside (the SZA beyond 100° in Figure 6) may be due to scattering by wave-particle interactions with photoelectrons traveling along magnetic field lines (Jasperse, 1977; Jasperse & Smith, 1978), as enhanced waves are found to reduce the particle anisotropy (Gary & Wang, 1996; Li et al., 2008). This may be the reason why the probability of near-isotropic photoelectrons is not always 0 at high altitudes where it is very unlikely that photoelectrons were produced locally.

The classification of the different types of photoelectron PAD is also associated with the $\alpha_{\mathrm{ani}}^{\mathrm{limit}}$ we use. We further analyze how the results may change with a different $\alpha_{\mathrm{ani}}^{\mathrm{limit}}$. In Figure 8, the top panel shows the ratio of near-isotropic photoelectron distributions to the total number of classified photoelectron peak detections in every 2,000-km height bin. We used different values of $\alpha_{\mathrm{ani}}^{\mathrm{limit}}$ from 2.0 to 4.0 to demonstrate the changes

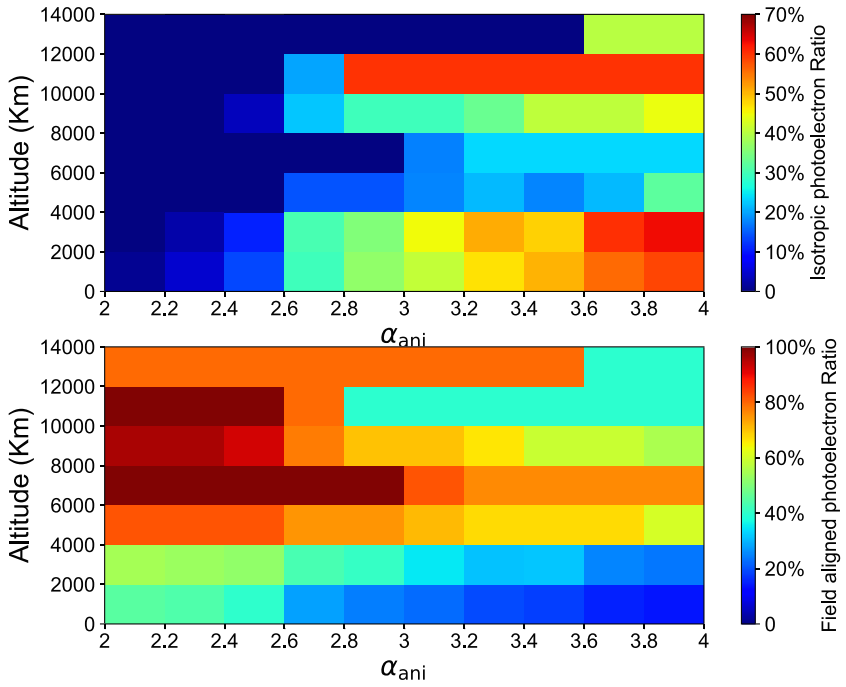

Figure 8. The ratio of near-isotropic photoelectron distributions (top panel) and field-aligned photoelectron distributions (bottom panel) to the total number of three categories of photoelectrons in every 2,000-km height bin with different threshold value of α_{ani}^{limit}. The color indicates the ratio of the particular type of photoelectrons.

of ratio at different heights. Below 4,000 km, the ratio of near-isotropic photoelectron distributions is sensitive to the change of α_{ani}^{limit}. With α_{ani}^{limit} increasing from 2.0 to 4.0, the ratio increases from almost 0 to over 50%. According to our study, 65% of the photoelectrons are seen in the dayside ionosphere, below 4,000 km. Because the locally produced photoelectrons are isotropic, the ratio of near-isotropic photoelectron distributions is sensitive to α_{ani}^{limit}, the criterion we use to classify near-isotropic photoelectron distributions. Above 4,000 km and below 8,000 km, the ratio of near-isotropic photoelectron distributions gradually increases by 30% when α_{ani}^{limit} increases from 2.0 to 4.0 because at this altitude range, the field-aligned photoelectrons become the dominant type. Above 8,000 km, the ratio of near-isotropic photoelectron becomes sensitive to the α_{ani}^{limit} again due to the limited number of observations. The observations of near-isotropic photoelectrons at that altitude may be produced by the scattering of magnetic field-aligned photoelectrons. The bottom panel is similar to the top one but shows the variation of the ratio of field-aligned photoelectron distributions with different α_{ani}^{limit}. Between 4,000 and 10,000 km, the ratio of field-aligned photoelectron distributions takes up over 60% and is not sensitive to the change of α_{ani}^{limit}. When α_{ani}^{limit} increases from 2.0 to 4.0, the ratio just changes by approximately 20%. Despite that the classification of photoelectrons somewhat depends on the choice of α_{ani}^{limit}, the main conclusion of the paper, in terms of the trend to observe field-aligned photoelectrons at high altitudes, is significant.

5. Conclusions

Previous research on photoelectron peaks from the CAPS-ELS showed that some photoelectrons observed at large distances from Titan indicate the escape of photoelectrons from Titan's day ionosphere along magnetic field (e.g., Coates et al., 2007; Wellbrock et al., 2012). In this work, we use an automatic finite impulse response algorithm to detect all photoelectron signatures from the ELS data during 56 Titan flybys and use the result to present the spatial distribution of photoelectrons. Most of the photoelectrons are observed in the sunlit ionosphere, but some are also found in the dark-side of Titan or extend to high altitudes. We identified a gap of photoelectrons in the dark-side of Titan's ionosphere over the altitude range of 950–2,700 km and with SZA > 130°. The gap region was sampled by more than 20 flybys; however, only two photoelectron peaks were detected. It appears to be very difficult for photoelectrons to travel to this particular combination of altitude and SZAs (the gap region) from the dayside ionosphere, and this does not appear to change

for different magnetospheric conditions. Considering the different orientations of the solar and corotation wakes of Titan does not help to explain the presence of this gap region.

We defined a parameter α_{ani} to classify near-isotropic photoelectrons and found that the probability of finding field-aligned photoelectrons at high altitude (>4,000 km) is significantly higher than finding non-field-aligned photoelectrons. Similarly, field-aligned photoelectrons are significantly more abundant on the dark-side at SZA > 100°. These survey results are consistent with the prediction that photoelectrons found at high altitude or on the nightside traveled along magnetic field lines from the sunlit ionosphere, where they were produced. Some near-isotropic photoelectron observations on the nightside ionosphere and at high altitude are expected to be caused by wave-particle interactions, which can reduce the anisotropy of particles. More detailed case studies together with modeling efforts are clearly required to interpret the photoelectron gap region and the observations of near-isotropic photoelectron distributions at high altitudes and at large SZA.

Acknowledgments
We acknowledge support by the UK Science and Technology Facilities Council consolidated Grant ST/S000240/1. R. C. acknowledges support by Ministerio de Economía y Competitividad of Spain (Project ESP2016-79135-R). M. G. acknowledges support by STFC of UK under Grant ST/N000692/4. J. C. acknowledges supports from the National Science Foundation of China through Grants 41525015 and 41774186. Y.-T. C. acknowledges the scholarship offered by UCAS to participate in a Joint PhD Training Program in UK. Cassini CAPS-ELS data are available at the NASA Planetary Data System and were processed using MSSL's Cassini data analysis system. All photoelectron identification results can be accessed via Caro-Carretero, Raquel; Wellbrock, Anne; Cao, Yutian (2019), "Cassini ELS Photoelectron identification," Mendeley Data, v1 (https://doi.org/10.17632/dwxhzbnvr9.1).

References

Ågren, K., Wahlund, J.-E., Garnier, P., Modolo, R., Cui, J., Galand, M., & Müller-Wodarg, I. (2009). On the ionospheric structure of Titan. *Planetary and Space Science*, *57*, 1821–1827. https://doi.org/10.1016/j.pss.2009.04.012

Agren, K., Wahlund, J.-E., Modolo, R., Lummerzheim, D., Galand, M., Müller-Wodarg, I., et al. (2007). On magnetospheric electron impact ionisation and dynamics in Titan's ram-side and polar ionosphere—A Cassini case study. *Annales Geophysicae*, *25*, 2359–2369. https://doi.org/10.5194/angeo-25-2359-2007

Allen, R. V. (1978). Automatic earthquake recognition and timing from single traces. *Bulletin of the Seismological Society of America*, *68*(5), 1521–1532.

Allen, R. V. (1982). Automatic phase pickers: Their present use and future prospects. *Bulletin of the Seismological Society of America*, *72*, S225–S242.

Backes, H., Neubauer, F. M., Dougherty, M. K., Achilleos, N., André, N., Arridge, C. S., et al. (2005). Titan's magnetic field signature during the first Cassini encounter. *Science*, *308*, 992–995. https://doi.org/10.1126/science.1109763

Bertucci, C., Achilleos, N., Dougherty, M. K., Modolo, R., Coates, A. J., Szego, K., et al. (2008). The magnetic memory of Titan's ionized atmosphere. *Science*, *321*, 1475. https://doi.org/10.1126/science.1159780

Bertucci, C., Hamilton, D. C., Kurth, W. S., Hospodarsky, G., Mitchell, D., Sergis, N., et al. (2015). Titan's interaction with the supersonic solar wind. *Geophysical Research Letters*, *42*, 193–200. https://doi.org/10.1002/2014GL062106

Bridge, H. S., Belcher, J. W., Lazarus, A. J., Olbert, S., Sullivan, J. D., Bagenal, F., et al. (1981). Plasma observations near Saturn—Initial results from Voyager 1. *Science*, *212*, 217–224. https://doi.org/10.1126/science.212.4491.217

Coates, A. J. (2009). Interaction of Titan's ionosphere with Saturn's magnetosphere. *Philosophical Transactions of the Royal Society of London Series A*, *367*, 773–788. https://doi.org/10.1098/rsta.2008.0248

Coates, A. J., Crary, F. J., Young, D. T., Szego, K., Arridge, C. S., Bebesi, Z., et al. (2007). Ionospheric electrons in Titan's tail: Plasma structure during the Cassini T9 encounter. *Geophysical Research Letters*, *34*, L24S05. https://doi.org/10.1029/2007GL030919

Coates, A. J., Frahm, R. A., Linder, D. R., Kataria, D. O., Soobiah, Y., Collinson, G., et al. (2008). Ionospheric photoelectrons at venus: Initial observations by ASPERA-4 ELS. *Planetary and Space Science*, *56*, 802–806. https://doi.org/10.1016/j.pss.2007.12.008

Coates, A. J., Johnstone, A. D., Sojka, J. J., & Wrenn, G. L. (1985). Ionospheric photoelectrons observed in the magnetosphere at distances up to 7 Earth radii. *Planetary and Space Science*, *33*, 1267–1275. https://doi.org/10.1016/0032-0633(85)90005-4

Coates, A. J., Tsang, S. M. E., Wellbrock, A., Frahm, R. A., Winningham, J. D., Barabash, S., et al. (2011). Ionospheric photoelectrons: Comparing Venus, Earth, Mars and Titan. *Planetary and Space Science*, *59*, 1019–1027. https://doi.org/10.1016/j.pss.2010.07.016

Coates, A. J., Wellbrock, A., Frahm, R. A., Winningham, J. D., Fedorov, A., Barabash, S., & Lundin, R. (2015). Distant ionospheric photoelectron energy peak observations at Venus. *Planetary and Space Science*, *113*, 378–384. https://doi.org/10.1016/j.pss.2015.02.003

Coates, A. J., Wellbrock, A., Waite, J. H., & Jones, G. H. (2015). A new upper limit to the field-aligned potential near Titan. *Geophysical Research Letters*, *42*, 4676–4684. https://doi.org/10.1002/2015GL064474

Cravens, T. E., Richard, M., Ma, Y.-J., Bertucci, C., Luhmann, J. G., Ledvina, S., et al. (2009). Model-data comparisons for Titan's nightside ionosphere. *Journal of Geophysical Research*, *115*, A08319. https://doi.org/10.1029/2009JA015050

Cravens, T. E., Robertson, I. P., Waite, J. H., Yelle, R. V., Vuitton, V., Coates, A. J., et al. (2009). Model-data comparisons for Titan's nightside ionosphere. *Icarus*, *199*, 174–188. https://doi.org/10.1016/j.icarus.2008.09.005

Cui, J., Galand, M., Coates, A. J., Zhang, T. L., & Müller-Wodarg, I. C. F. (2011). Suprathermal electron spectra in the Venus ionosphere. *Journal of Geophysical Research*, *116*, A04321. https://doi.org/10.1029/2010JA016153

Cui, J., Galand, M., Yelle, R. V., Vuitton, V., Wahlund, J. E., Lavvas, P. P., et al. (2009). Diurnal variations of Titan's ionosphere. *Journal of Geophysical Research*, *114*, A06310. https://doi.org/10.1029/2009JA014228

Cui, J., Yelle, R. V., Strobel, D. F., Müller-Wodarg, I. C. F., Snowden, D. S., Koskinen, T. T., & Galand, M. (2012). The CH_4 structure in Titan's upper atmosphere revisited. *Journal of Geophysical Research*, *117*, E11006. https://doi.org/10.1029/2012JE004222

Cui, J., Yelle, R. V., Vuitton, V., Waite, J. H., Kasprzak, W. T., Gell, D. A., et al. (2009). Analysis of Titan's neutral upper atmosphere from Cassini Ion Neutral Mass Spectrometer measurements. *Icarus*, *200*, 581–615. https://doi.org/10.1016/j.icarus.2008.12.005

Dougherty, M. K., Kellock, S., Southwood, D. J., Balogh, A., Smith, E. J., Tsurutani, B. T., et al. (2004). The Cassini magnetic field investigation. *Space Science Reviews*, *114*(1-4), 331–383. https://doi.org/10.1007/s11214-004-1432-2

Frahm, R. A., Winningham, J. D., Sharber, J. R., Scherrer, J. R., Jeffers, S. J., Coates, A. J., et al. (2006). Carbon dioxide photoelectron energy peaks at Mars. *Icarus*, *182*(2), 371–382. https://doi.org/10.1016/j.icarus.2006.01.014

Galand, M., Coates, A. J., Cravens, T. E., & Wahlund, J.-E. (2014). Titan's ionosphere (p. 376).

Galand, M., Yelle, R. V., Coates, A. J., Backes, H., & Wahlund, J.-E. (2006). Electron temperature of Titan's sunlit ionosphere. *Geophysical Research Letters*, *33*, L21101. https://doi.org/10.1029/2006GL027488

Galand, M., Yelle, R., Cui, J., Wahlund, J.-E., Vuitton, V., Wellbrock, A., & Coates, A. (2010). Ionization sources in Titan's deep ionosphere. *Journal of Geophysical Research*, *115*, A07312. https://doi.org/10.1029/2009JA015100

Gary, S. P., & Wang, J. (1996). Whistler instability: Electron anisotropy upper bound. *Journal of Geophysical Research*, *101*, 10,749–10,754. https://doi.org/10.1029/96JA00323

Hartle, R. E., Sittler, E. C., Neubauer, F. M., Johnson, R. E., Smith, H. T., Crary, F., et al. (2006). Preliminary interpretation of Titan plasma interaction as observed by the Cassini plasma spectrometer: Comparisons with Voyager 1. *Geophysical Research Letters*, *33*, L08201. https://doi.org/10.1029/2005GL024817

Jasperse, J. R. (1977). Electron distribution function and ion concentrations in the Earth's lower ionosphere from Boltzmann-Fokker-Planck theory. *Planetary and Space Science*, *25*, 743–756. https://doi.org/10.1016/0032-0633(77)90126-X

Jasperse, J. R., & Smith, E. R. (1978). The photoelectron flux in the Earth's ionosphere at energies in the vicinity of photoionization peaks. *Geophysical Research Letters*, *5*, 843–846. https://doi.org/10.1029/GL005i010p00843

Lewis, G. R., André, N., Arridge, C. S., Coates, A. J., Gilbert, L. K., Linder, D. R., & Rymer, A. M. (2008). Derivation of density and temperature from the Cassini Huygens CAPS electron spectrometer. *Planetary and Space Science*, *56*, 901–912. https://doi.org/10.1016/j.pss.2007.12.017

Lewis, G. R., Arridge, C. S., Linder, D. R., Gilbert, L. K., Kataria, D. O., Coates, A. J., et al. (2010). The calibration of the Cassini-Huygens CAPS electron spectrometer. *Planetary and Space Science*, *58*, 427–436. https://doi.org/10.1016/j.pss.2009.11.008

Li, W., Thorne, R. M., Meredith, N. P., Horne, R. B., Bortnik, J., Shprits, Y. Y., & Ni, B. (2008). Evaluation of whistler mode chorus amplification during an injection event observed on CRRES. *Journal of Geophysical Research*, *113*, A09210. https://doi.org/10.1029/2008JA013129

Linder, D. R., Coates, A. J., Woodliffe, R. D., Alsop, C., Johnstone, A. D., Grande, M., et al. (1998). The Cassini CAPS electron spectrometer. *Washington DC American Geophysical Union Geophysical Monograph Series*, *102*, 257. https://doi.org/10.1029/GM102p0257

Liu, X., & Shemansky, D. E. (2006). Analysis of electron impact ionization properties of methane. *Journal of Geophysical Research*, *111*, A04303. https://doi.org/10.1029/2005JA011454

Ma, Y. J., Russell, C. T., Nagy, A. F., Toth, G., Bertucci, C., Dougherty, M. K., et al. (2009). Time-dependent global MHD simulations of Cassini T32 flyby: From magnetosphere to magnetosheath. *Journal of Geophysical Research*, *114*, A03204. https://doi.org/10.1029/2008JA013676

Mantas, G. P., & Hanson, W. B. (1979). Photoelectron fluxes in the Martian ionosphere. *Journal of Geophysical Research*, *84*, 369–385. https://doi.org/10.1029/JA084iA02p00369

Nagy, A. F., & Banks, P. M. (1970). Photoelectron fluxes in the ionosphere. *Journal of Geophysical Research*, *75*, 6260–6270. https://doi.org/10.1029/JA075i031p06260

Ness, N. F., Acuna, M. H., Behannon, K. W., & Neubauer, F. M. (1982). The induced magnetosphere of Titan. *Journal of Geophysical Research*, *87*, 1369–1381. https://doi.org/10.1029/JA087iA03p01369

Neubauer, F. M., Gurnett, D. A., Scudder, J. D., & Hartle, R. E. (1984). Titan's magnetospheric interaction.

Regoli, L. H., Coates, A. J., Thomsen, M. F., Jones, G. H., Roussos, E., Waite, J. H., et al. (2016). Survey of pickup ion signatures in the vicinity of Titan using CAPS/IMS. *Journal of Geophysical Research: Space Physics*, *121*, 8317–8328. https://doi.org/10.1002/2016JA022617

Schunk, R. W., & Nagy, A. F. (2000). *Planetary ionospheres*, Cambridge Atmospheric and Space Science Series (pp. 433–463). Cambridge: Cambridge University Press. https://doi.org/10.1017/CBO9780511551772.013

Sillanpää, I., Kallio, E., Janhunen, P., Schmidt, W., Mursula, K., Vilppola, J., & Tanskanen, P. (2006). Hybrid simulation study of ion escape at Titan for different orbital positions. *Advances in Space Research*, *38*, 799–805. https://doi.org/10.1016/j.asr.2006.01.005

Strobel, D. F. (2012). Hydrogen and methane in Titan's atmosphere: Chemistry, diffusion, escape, and the Hunten limiting flux principle (this article is part of a special issue that honours the work of Dr. Donald M. Hunten FRSC who passed away in December 2010 after a very illustrious career). *Canadian Journal of Physics*, *90*(8), 795–805. https://doi.org/10.1139/p11-131

Tsang, S. M. E., Coates, A. J., Jones, G. H., Frahm, R. A., Winningham, J. D., Barabash, S., et al. (2015). Ionospheric photoelectrons at Venus: Case studies and first observation in the tail. *Planetary and Space Science*, *113*, 385–394. https://doi.org/10.1016/j.pss.2015.01.019

Wahlund, J.-E., Boström, R., Gustafsson, G., Gurnett, D., Kurth, W., Pedersen, A., et al. (2005). Cassini measurements of cold plasma in the ionosphere of Titan. *Science*, *308*(5724), 986–989.

Wei, H. Y., Russell, C. T., Wahlund, J.-E., Dougherty, M. K., Bertucci, C., Modolo, R., et al. (2007). Cold ionospheric plasma in Titan's magnetotail. *Geophysical Research Letters*, *34*, L24S06. https://doi.org/10.1029/2007GL030701

Wellbrock, A., Coates, A. J., Sillanpää, I., Jones, G. H., Arridge, C. S., Lewis, G. R., et al. (2012). Cassini observations of ionospheric photoelectrons at large distances from Titan: Implications for Titan's exospheric environment and magnetic tail. *Journal of Geophysical Research*, *117*, A03216. https://doi.org/10.1029/2011JA017113

Xu, S., Mitchell, D., Liemohn, M., Dong, C., Bougher, S., Fillingim, M., et al. (2016). Deep nightside photoelectron observations by MAVEN SWEA: Implications for Martian northern hemispheric magnetic topology and nightside ionosphere source. *Geophysical Research Letters*, *43*, 8876–8884. https://doi.org/10.1002/2016GL070527

Xu, S., Mitchell, D., Liemohn, M., Fang, X., Ma, Y., Luhmann, J., et al. (2017). Martian low-altitude magnetic topology deduced from MAVEN/SWEA observations. *Journal of Geophysical Research: Space Physics*, *122*, 1831–1852. https://doi.org/10.1002/2016JA023467

Xu, S., Mitchell, D., Luhmann, J., Ma, Y., Fang, X., Harada, Y., et al. (2017). High-altitude closed magnetic loops at Mars observed by MAVEN. *Geophysical Research Letters*, *44*, 11,229–11,238. https://doi.org/10.1002/2017GL075831

Young, D. T., Berthelier, J. J., Blanc, M., Burch, J. L., Coates, A. J., Goldstein, R., et al. (2004). Cassini plasma spectrometer investigation. *Space Science Reviews*, *114*, 1–112. https://doi.org/10.1007/s11214-004-1406-4